Influences of fuel bed depth and air supply on small-scale batch-fed reverse downdraft biomass conversion

Thomas Kirch,[*,†,‡] Paul R. Medwell,[†,‡] Cristian H. Birzer,[†,‡] and Philip J. van Eyk[¶,‡]

†*School of Mechanical Engineering, The University of Adelaide, Australia*

‡*Humanitarian and Development Solutions Initiative, The University of Adelaide, Australia*

¶*School of Chemical Engineering, The University of Adelaide, Australia*

E-mail: thomas.kirch@adelaide.edu.au

Abstract

The producer gas composition and the thermochemical conversion process of a small-scale reverse downdraft reactor has been investigated under ten operating conditions with different fuel bed depths and air supply rates. The operating principle of this research reactor is a batch-fed reverse downdraft process, using wood pellets as the solid biomass fuel. The oxygen-limited regime, where the fuel consumption increases nearly linearly with the air supply, has been identified and four flow rates over the range of this regime have been investigated. The fuel bed depth was varied between one and four reactor diameters (1D (100 mm) – 4D (400 mm)). The results demonstrate that increasing the primary air mass flux leads to both greater fuel consumption and higher temperatures as well as heating rates in the reaction front. Greater air supply rates and the resulting higher temperatures lead to a substantial increase in fuel conversion into permanent gases, rather than tars or char, and a rise in

the cold gas efficiency (CGE) from 33 to 73%, from the lowest to highest air flow rate at a 4D fuel bed depth. However, the temporal producer gas heating value is similar in all configurations. With increasing depth, it is evident that H_2 production is promoted by the char layer downstream of the reaction front and that a certain layer thickness is necessary to achieve the potential near steady-state product flow at a specific flow rate. Interestingly, a greater fuel bed depth enhances the hydrogen conversion rate to permanent gases by more than 20% and the CGE from 48 to 53%, while the fuel consumption and temperature profiles remain similar. A general trend of increasing performance was identified at the 3D and 4D depths, when compared with the 1D and 2D fuel bed depths. The produced char exhibits a high fixed and elemental carbon content. Therefore, the conversion efficiency of this process can be increased both through increasing the fuel bed depth and, even more, through adjusting the air supply, promoting the yield of permanent gases and the conversion of produced tars.

1 Introduction

Solid biomass fuels provide the majority of renewable energy worldwide[1] and are often used in small-scale devices for localised heat generation. Unfortunately, current small-scale devices typically have low efficiency and high emissions of incomplete combustion.[2] An alternative reactor type features reverse downdraft, whereby the thermochemical conversion process of the solid biomass fuel is separated in time and location from the combustion of the product gas. These types of reactors achieve lower emissions of incomplete combustion,[3] and show potential for small-scale heat and power generation.[4,5] However, despite the potential applications, a deeper understanding of the ongoing thermochemical conversion processes in such systems is needed for the systematic improvement of future designs.[6]

Packed-bed reverse downdraft reactors are lit from the top, which leads to the ignition of the surface of the solid fuel, while air is supplied from underneath the fuel bed.[7] Subsequently, a reaction front propagates against the air flow, down the fuel bed, causing the release of volatile matter and leaving a solid layer of char.[8] The devolatilisation process in the reaction front is sustained by heat from partial oxidation of the volatile gases with the limited air supply and is therefore called an autothermal process.[9] The gaseous products ("producer gas") rise through the solid layer of hot char, leave the fuel bed and can subsequently be burned with secondary air.[10,11] Once the reaction front reaches the bottom of the fuel bed, the majority of the volatile matter has been released and char, consisting mainly of fixed carbon, is left as a solid product.[12] At this stage, the process can be quenched and the char can be collected. If the process is not quenched, an updraft process starts where the char is oxidised, with the air supply from underneath. This can release high concentrations of CO. The process continues until only the ash is left behind as a solid product. If the process is quenched before the updraft process starts, the char product can be collected and used for other purposes, depending on its properties. In order to increase the quality, quantity and range of application of the char, it is necessary to

further develop understanding and optimisation of the process for producer gas as well as char production.[13]

For batch-fed systems, three combustion regimes have been identified, with increasing air supply: (1) an oxygen-limited regime, where the fuel consumption is nearly linearly dependent on the oxidiser supply; (2) a reaction-limited regime, where the solid fuel mass loss is independent of the air flow rate; and (3) a regime where the process is cooled by convection and finally quenched.[14] The limits of these regimes are fuel dependent and are influenced by characteristics such as the fuel moisture content and particle size.[15–18] In the oxygen-limited regime, the conversion process is controlled by the air supply, thereby enabling the heat release via this parameter. Small-scale reverse downdraft reactors mostly operate in the oxygen-limited regime, but limited research has been concerned with the products of the thermochemical conversion process released under these conditions: instead the focus has primarily been on the air supply and the overall system performance, including the subsequent combustion process.[3]

With limited air supply, the products of the devolatilisation process are: (1) a wide variety of gases (CO, CO_2, H_2, CH_4 C_2H_2, C_2H_4, C_2H_6, C_6H_6, etc.);[19] (2) liquid tars, heavier hydrocarbons, and water; and (3) solid char (mostly carbon and ash). The producer gas composition (on a volumetric basis) of batch-fed autothermal gasification has been reported in the range of 1–9% H_2, 8–13% CO, 11–20% CO_2 and 1–3% CH_4.[20,21] The main factors influencing producer gas composition are the air supply, heating rate, final temperature and the type of initial biomass fuel,[22] coupled with the design and pressure of the reactor.[9] The fuel bed depth as a design parameter is not well understood and could be influential on the producer gas composition.

While the gaseous and solid devolatilisation products are desired, the liquid products, and especially the tars, are generally not desired, since these hydrocarbon compounds have been identified as soot precursors.[23] In the reverse downdraft configuration, the hot temperatures and catalytic properties of char downstream of the reaction front can influ-

ence those products that are released from the devolatilisation process. While maximum reaction temperatures are dependent on the air supply, the char layer thickness above the reaction front increases as the reaction propagates down the fuel bed. Thermal cracking (decomposition) reactions of tars released from biomass pyrolysis have been shown to increase with temperature[24,25] and can achieve 80–90% tar reduction at temperatures above 1000°C.[26] Primary and secondary tars have been reduced at temperatures over 1100°C, due to cracking reactions, although more tertiary tars are formed.[26–28] Thermal tar cracking reactions are expected to increase the production of CO and H_2.[28] These reactions can be enhanced in the presence of char,[19,29–31] which can lead to a further reduction of tar after the released products pass through a hot char bed.[32] The maximum char layer thickness is dependent on the initial fuel bed depth as it increases with the propagation of the reaction front. It has been suggested that cracking processes due to the presence of char are limited in small-scale reverse downdraft reactors because of the limited thickness of the char layer.[33] A variation of the air supply and the fuel bed depth, can therefore yield further insights into the effects of thermal cracking and the presence of a hot char layer on the composition of the producer gas in reverse downdraft reactors.

This research article aims to contribute to a deeper understanding and further classification of the ongoing processes in small-scale batch-fed reverse downdraft reactors. Two parameters, the fuel bed depth and the air supply rate are investigated. While the air flow rate has previously been identified as reaction limiting at low supply rates, the influence of the fuel bed depth has not yet been extensively studied and further information can be gained from an in depth analysis of the products released from the thermochemical conversion process. A combined study of both parameters allows a comparison and determination of the degree to which the fuel bed depth and the air supply influence the released products. Producer gas, as well as solid char, are considered as products and their properties are investigated through an analysis of their composition. The findings of this work could provide alternative means by which to analyse reactor designs in terms

of process optimisation for the combined production of producer gas and char.

2 Experimental Setup

2.1 Reactor

A schematic diagram of the batch-fed reactor is presented in Figure 1. Fuel was loaded from the top and placed on a grate mounted above an air plenum. For this arrangement, the air entering from the bottom was purposely insufficient to oxidise all the producer gas within the length of the reactor. A small portion of the released gases from the devolatilisation process were extracted from the reactor, and the remainder were subsequently combusted in a non-premixed flame immediately above the exit plane of the reactor. It is important to note that the measurements are sampled from within the potential core of the jet, upstream of the flame, and are not influenced by the secondary combustion process.

The supply of dry compressed air was regulated through a flow meter and introduced into the reactor via a distribution ring, with its nozzles facing downwards to create an even flow pattern. Based on preliminary experiments to span the combustion regimes of interest, air mass fluxes of 0.025, 0.050, 0.075 and 0.125 $\mathrm{kg{\cdot}m^{-2}{\cdot}s^{-1}}$ were chosen for the present study. For simplicity, these flow rates will be referred to as FR025, FR050, FR075 and FR125 from here on.

Up to eight K-type thermocouples (labelled T1–T8) are inserted into the fuel. Thermocouple 1 was mounted at a distance of 30 mm beneath the initial top of the fuel bed, with distances of 50 mm between each of the subsequent thermocouples, while the last thermocouple was placed at 20 mm above the fuel grate. The reactor was mounted on a weighing scale (Radwag WLC 20/A2) with a maximum capacity of 20.0 kg, with a readability and repeatability of 10^{-4} kg.

The reactor has an inner diameter of 98 mm. The external wall was covered with 25-

mm-thick thermal insulation. The grate has a 67.2% open area and adjustable feet, so that its location can be adjusted within the reactor to accommodate diverse fuel bed heights between 100 and 400 mm. In all cases, the top of the fuel stack was always initially at the entrance plane of the extraction probe.

An extraction probe, for sampling the released devolatilisation products, was situated at the top of the fuel bed. The probe consists of a 90° bend before penetrating the reactor wall, leading into a heated line which was subsequently introduced into a cooled tar trap. The tar trap was used for the retention of all non-gaseous products. A feasible method for the gravimetric measurement of the produced tars could not be established in the research facilities. Downstream of the tar trap, an adjustable flow rate vacuum pump regulated the flow of sample extraction and was manually set to correspond to the gas analyser flow rate. Subsequently, the flow passes through the gas analyser (§2.2).

2.2 Gas Analyser

The gas analyser downstream of the tar trap was an MRU Vario Plus Industrial Analyser, which measures volumetric composition on a dry basis. CO_2, CO and C_xH_y, reported as a CH_4 equivalent, are measured using NDIR sensors with a range up to 30% (mol/mol) and an accuracy $\pm$ 3% of the reading. O_2 and H_2 are measured using an electrochemical sensor with a range up to 21% and an accuracy of $\pm$ 0.2% of the absolute value, and a range up to 100% and an accuracy $\pm$ 0.02% of the reading, respectively. CO_2, CO, CH_4, H_2 and O_2 are measured by the analyser, with N_2 determined by subtraction . Calibration of the gas analyser was performed daily. Measurements were recorded continuously at a rate of 0.5 Hz.

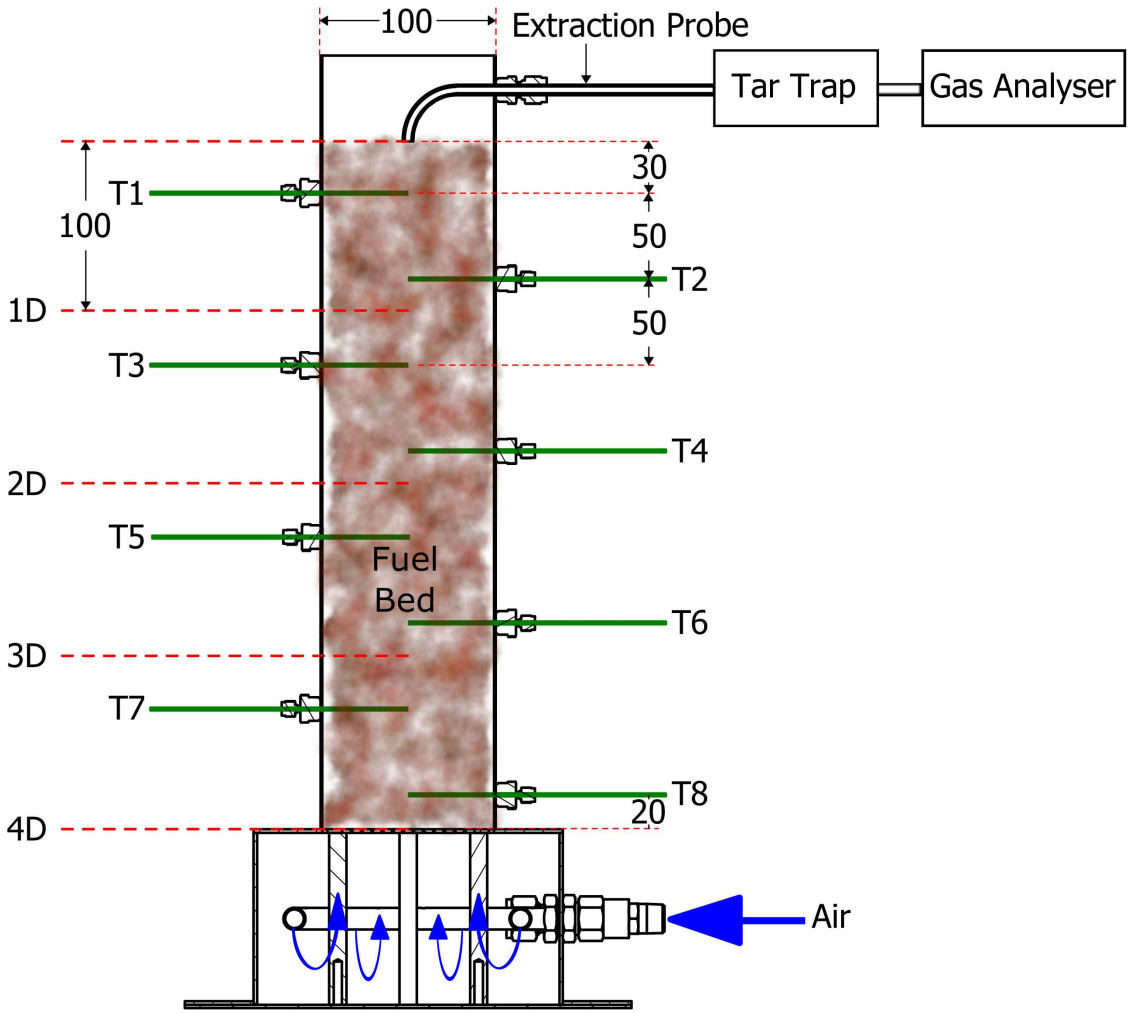

Figure 1: Schematic diagram of the reactor and measuring equipment set-up. All distances in millimetres.

2.3 Fuel

Cylindrical wood pellets, with a nominal diameter of 6.5 mm and nominal length of 40 mm (resulting in 5–40 mm length), produced from timber waste in multiple timber mills around Australia, were used as fuel. The pellets consist of hammer-milled wood shavings, from multiple wood species, to which pine saw dust is added before being compressed, resulting in a bulk density of approximately 700 $kg \cdot m^{-3}$. Pellet Heaters Australia manufacture the product which, was purchased from Barbeques Galore (Adelaide, Australia). The proximate analysis of the pellets yielded a dry-basis mass composition of

76.5% volatile matter, 17.6% char, and 5.9% ash. The moisture content of the raw fuel was 4.3% (g/g), using an established method.[34] The mass-based ultimate analysis resulted in 47.4% C, 6.4% H and 0.1% N and the higher heating value of the fuel was 17.6 $MJ \cdot kg^{-1}$, as determined in a bomb calorimeter.

2.4 Procedure

Two main parameters, the air mass flux and the fuel bed depth, were controlled in the present study, as presented in Table 1. To avoid any influence from the thermal mass of the reactor (cold start) on the process, it was preheated prior to use. Fuel was introduced into the reactor at inner reactor temperatures <100°C, to avoid an effect from fuel drying. For each experiment, the pre-weighed fuel batch was placed into the reactor and the air mass flux was pre-set on the flow meters. The top of the fuel bed was lit, with the aid of 10 mL of methylated spirits (96% ethanol, CAS # 67-63-0) and one paper towel for ignition, when the outer reactor wall was approximately 50°C.

When the reaction front reached the fuel grate the experiment was stopped. The end time was determined by calculating the average reaction front velocity (the distance over time between the thermocouples reaching 600°C) for each configuration, and extrapolating from the time after thermocouple T8 measured 600°C. The process was then stopped by shutting off the air supply and introducing one third of the estimated char mass as iced water into the reactor, to rapidly cool the process. To further quench all reactions, nitrogen (>99.99% N_2) was supplied through the air inlet at the bottom of the reactor and passed over the char layer.

Four fuel bed depth and four flow rates were tested, with each configuration being repeated multiple times, as presented in Table 1. The fuel bed depths of 100, 200, 300 and 400 mm are set in relation to the inner diameter of the reactor, 98 mm, and are referred to as 1D, 2D, 3D and 4D hereafter. At 1D and 4D four air flow rates were used, while all four depths were only tested at 0.075 $kg \cdot m^{-2} \cdot s^{-1}$. The clear trend established at 1D and

4D is consistent, and therefore it was not necessary to repeat measurements at 2D and 3D for all four flow rates.

After each test, the remaining char, as the solid product of the process, was extracted from the reactor. In the case of the 4D fuel bed depth, the remaining char was extracted in three distinct portions. The three portions describe the top, middle and bottom third of the char bed in the reactor.

Table 1: Experimental configurations, the number of repetitions performed and the experimental code.

Fuel bed depth (mm)	Fuel Mass (kg)	Air Mass Flux ($kg \cdot m^{-2} \cdot s^{-1}$)	Repetitions	Code
100	0.525	0.025	3	1D FR025
		0.050	3	1D FR050
		0.075	5	1D FR075
		0.125	3	1D FR125
200	1.05	0.075	6	2D FR025
300	1.575	0.075	5	3D FR025
400	2.1	0.025	5	4D FR025
		0.050	6	4D FR050
		0.075	5	4D FR075
		0.125	7	4D FR125

2.5 Analysis

A weighing scale was used to measure the fuel mass loss, which was expected to present a linear profile over time.[33] The measured weight loss confirmed the linear profile and a linear fit of the fuel mass flux was determined by the mass loss over time in relation to the cross-sectional area of the reactor. Preliminary data was gathered with a 1D fuel depth (0.525 kg of fuel) to establish the limits of the oxygen-limited air mass flux regime for the utilised fuel. The flow rates were increased into the reaction-limited regime to establish the limits of the oxygen-limited regime and the subsequent transition into the reaction-limited regime. In these preliminary experiments only weight loss data and temperature measurements were recorded. These results are compared with values from the

literature.[14] It should be kept in mind that the values found in the literature[14,16] were calculated on the basis of thermocouple data, represented by the reaction front velocity and the fuel bulk density ($\dot{m}_{fuel} = v_{front} \cdot \rho_{fuel}$) because the fuel mass loss was not measured. In this approximation, the remaining char was not considered and will therefore lead to an overestimation of the fuel mass flux, when compared with direct measurement of the fuel mass loss, as performed here.

A total of eight thermocouples, situated along the centre of the reactor, are measured via a thermocouple data logger. Mean maximum temperatures are determined as an average of the highest temperatures of the thermocouples used in the experiment. Maximum temperature measurements of the lowest thermocouple (20 mm from the fuel grate) were disregarded, since an influence of the temperature due to the proximity to the fuel grate was identified. For each thermocouple, the heating rate was calculated based on the time taken for the thermocouple to be heated from 100°C to 70% of the maximum temperature. The mean heating rate for each test was calculated from the heating rates of all the used thermocouples and the value reported for each configuration was the mean of all the repeat tests.

The producer gas composition was measured for the four different air mass flux rates at 1D and 4D, as well as for FR075 at 2D and 3D. Figure 2 presents a representative plot of one experiment (4D FR125), with the start and end points of the considered measurements. A uniform starting point had to be chosen, after which the profiles of multiple experiments provide similar trends. This enables the calculation of an average value for each time point after the starting point, leading to one average plot for each configuration. The O_2 concentration was chosen to determine the beginning and end points of the producer gas measurements. A threshold of 0.75% (vol/vol) O_2 was established as a reliable value. The start and end points of the measurement duration were determined when the O_2 concentration initially and at the end of the process passes this threshold, as shown in Figure 2. Mean values of the average plot for each configuration are calculated,

resulting in an average producer gas composition. The heating value of the producer gas was calculated on the basis of the higher heating value of the constituents. To calculate the product flow of gaseous species, N_2 was considered to be conserved. This takes into account that, since the amount of N_2 in the air supply and the concentration of N_2 in the producer gas was known, the amount of each gas species can be calculated from the molecular balance, as performed previously.[35] The continuous flow of products was calculated via Equation 1.

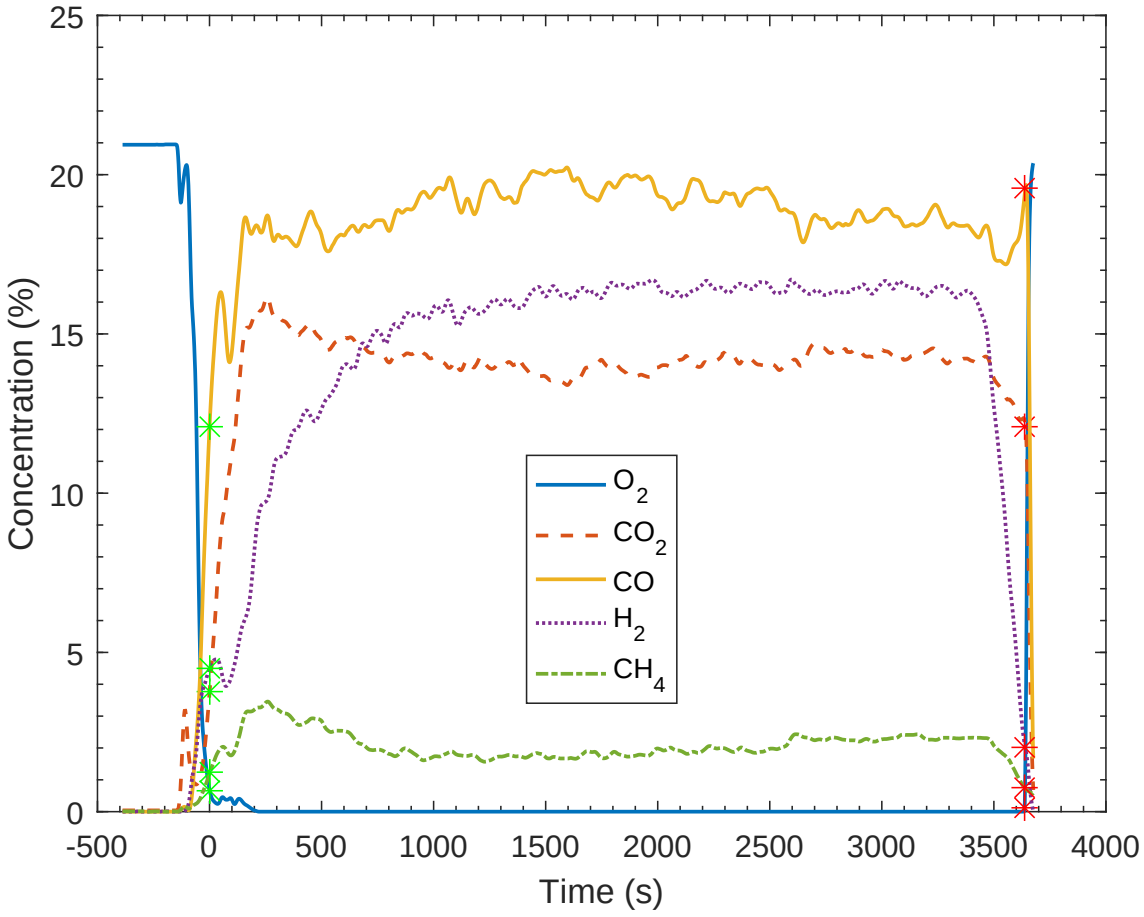

Figure 2: Example of volumetric concentration profiles of the continuous measurement of gaseous devolatilisation products at 4D FR125, with start and stop points marked by stars.

$$\dot{n}_{gas} = \frac{x_{gas}}{x_{N_2 measured}} \cdot \dot{n}_{N_2 air} \tag{1}$$

For the calculation of the fuel constituent conversion in the thermochemical conversion process, the supply of N_2 via air was considered to be conserved. The conversion of carbon and hydrogen from the fuel into the gas phase, as well as into specific gas species was determined by Equations 2 and 3.

$$C_{gas} = \frac{m_{air} \cdot \omega_{N_{air}} / M_{N_2} \cdot (x_{CO_2} + x_{CO} + x_{CH_4}) / x_{N_2}}{m_{fuel} \cdot \omega_C / M_C} \tag{2}$$

$$H_{2-gas} = \frac{m_{air} \cdot 0.767 / M_{N_2} \cdot (x_{H_2} + 2 \cdot x_{CH_4}) / x_{N_2}}{m_{fuel} \cdot \omega_H / M_H} \tag{3}$$

The cold gas efficiency, which describes the energy content of the producer gas relative to the energy content of the converted fuel, was calculated using Equation 4. This provides a measure of the loss of energy within the system, specifically the energy to sustain the autothermal process, heat loss from the reactor and latent heat of the products. As the energy contained in the char is not lost and available for subsequent processes it is subtracted from the energy of the provided fuel. The energy content of the producer gas was calculated based on the measured gas concentrations, while other hydrocarbon compounds, which are condensed in the tar trap and have not been quantified, are not included. The higher heating values (HHV) of the fuel and the char were measured using a bomb calorimeter, and those of the producer gas species were determined based on the composition measurements and using values reported in the literature.[36]

$$CGE = \frac{V_{N_2-air} / x_{N_2-measured} \cdot (x_{CO} \cdot 12.6 + x_{CH_4} \cdot 39.8 + x_{H_2} \cdot 12.8)}{HHV_{pellets} \cdot m_{fuel} - HHV_{char} \cdot m_{char}} \tag{4}$$

The biomass, along with the char samples from each configuration, were tested for their ultimate analysis (CHN composition), proximate analysis (moisture (M), volatile matter (VM), fixed carbon (FC) and ash content) and their HHV. The proximate analysis, using thermogravimetric analysis techniques, was based on a method previously reported.[34]

3 Results and Discussion

3.1 Mass Flux

The results of the mean fuel consumption rate as a function of the air supply are presented in Figure 3; both parameters are reported on a mass flux basis, and herein referred to as the fuel mass flux and the air mass flux. The error bars in Figure 3, as well as in all following figures, display the standard error of the mean.[37] As outlined in Section 1, in this type of reactor, three fuel mass flux regimes can be defined as a function of the air mass flux. The focus of the current work is on the oxygen-limited regime. Preliminary experiments were performed at one fuel bed depth (1D). Only the weight loss and temperature measurements were recorded in order to identify the upper-limit of the air mass flux (as described in §2.5), and are shown in Figure 3, where they are compared with those values reported in the literature.[14] More detailed experiments were performed at other fuel bed depths (1D–4D) and the gaseous product composition data were also collected and are presented in Figure 3. Further information on the stoichiometry of the process are provided in the Supporting Information.

In the oxygen-limited regime, the fuel mass flux increases linearly with the air mass flux, which Figure 3 indicates is for an air mass flux of $\lesssim$0.1 kg·m^{-2}·s^{-1} (up to approximately FR100). This range is in agreement with the literature for wood pellets.[14,16,38,39] Also apparent from Figure 3 is that the linear relationship between air and fuel mass flux is independent of the fuel stack depth (between 1D and 4D). A transition from the oxygen-limited to the reaction-limited regime is apparent around FR125, beyond which the fuel mass flux is nearly independent of the additional air supply. In the present study, the air mass flux was not further increased into the third regime (cooling), since in small-scale applications low air supplies are dominant. The ability to control the conversion process and heat release via the air supply is of particular interest here.

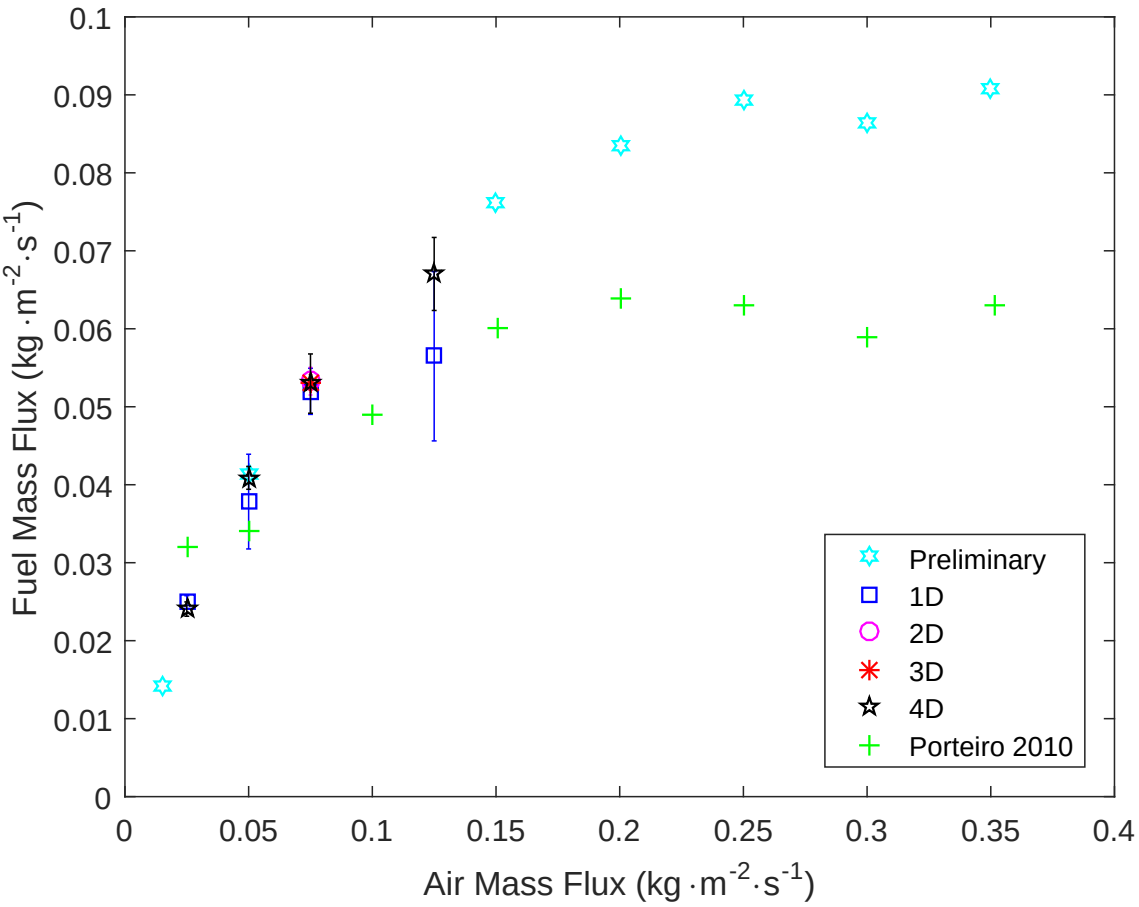

Figure 3: The fuel mass flux versus air mass flux for different experimental configurations, preliminary data and data found in the literature.[14] Error bars display the standard error of the mean.

3.2 Reactor Temperature

In Figure 4, the heating rate and the maximum reaction front temperature of the packed bed at the centre of the reactor are presented (calculated as presented in §2.5). In this figure the greater heat release at larger air supply rates is confirmed, as the mean maximum temperature as well as the heating rate increase with the air mass flux. A nearly linear increase of the mean maximum temperature of approximately 35% is noted over the five-fold increase in air mass flux, while the heating rate more than quadruples. As with the mass loss data (§3.1), the mean maximum temperature increases linearly for the air flow rates FR025–FR075.

Increasing temperatures have multiple influences on the process, as presented in §1. At temperatures greater than 1000°C, low tar yields are generally expected.[40] It has previously been described that particles undergoing devolatilisation have slightly lower temperature than that measured in the backed bed, because oxidation of the volatiles occurs in the gas phase surrounding the particle.[41,42] Therefore, the heating rate of the embedded thermocouples presented in Figure 4 is that of the packed bed, which will be similar to that of the particle itself. Therefore, the higher temperatures and heating rates in Figure 4 occur with the higher air flux cases FR075 and FR125, and thus these cases are expected to have lower tar yields.

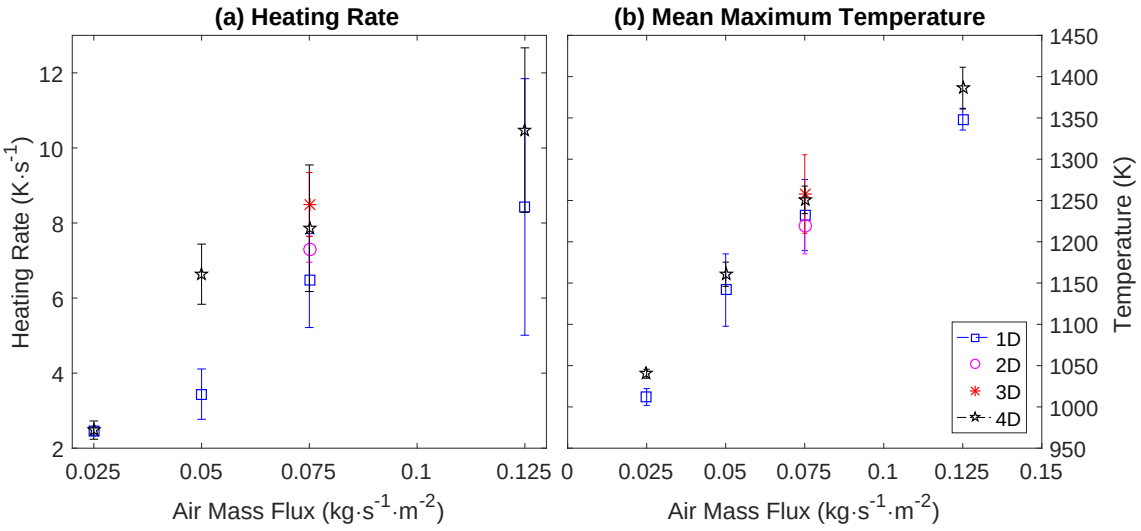

Figure 4: Heating rate (a) and mean maximum temperature (b) over the air mass flux. Error bars indicate the standard error of the mean.

3.3 Influence of air supply

3.3.1 Gaseous Products

In autothermal reactors the fuel mass flux, the temperature profiles and the producer gas composition are coupled, and dependent on the supplied air mass flux. In Figure 5 the molecular flow of the measured gaseous products (CO_2, CO, H_2, and CH_4) released over the duration of the process is presented. These products result from reactions in

the reaction front and downstream before reaching the extraction probe. Possible reactions are presented in Table 2. In the reaction front, while oxygen is available, exothermic reactions R1–R7 will be most influential and lead to substantial heat release. Once the oxygen is consumed and higher concentrations of CO_2 and H_2O (from combustion and fuel drying) are present, reactions R8–R15 will have a greater impact and the gas composition exiting the reaction front will depend on the thermochemical interaction between the presented reactions at the process temperature. As the reaction front moves down the fuel bed, along the temporal axis, more char is accumulated downstream of the front. While the devolatilisation products are released from the biomass and char is formed, the solid weight decreases but there is only minimal change in the occupied volume in the reactor. Therefore, for example, when half the duration of the process has passed, the products from the reaction front move through approximately half the initial fuel bed depth of char. Thus changes over time of released products can be related to an increasing char layer thickness, downstream of the reaction front, and ongoing reactions in this char layer. In Figure 5 the two main influences investigated in this article—the fuel bed depth and the air mass flux—are presented with all the flow rates for 1D and 4D cases. The plot for each configuration is an average of multiple repetitions of the experiment, as described in Section 2.5.

When changing the flow rates, FR025–FR125, at 1D and 4D depths, a complex influence on the different gaseous products is identified, in Figure 5. In all cases it can be seen that the flow of the measured gaseous species increases initially until it reaches a near steady-state flow. There is a gradual increase of product flow with increasing air flow. The well known increasing of the CO/CO_2 primary product ratio with increasing temperatures[45] can be noticed in the oxygen-limited regime (FR025–FR075) and is much more defined in the transition to the reaction-limited regime (FR125).

The release of CH_4 does not seem to follow the clear trend of increasing flow at higher air supplies. There is no notable flow increase between FR050–FR075, which suggests that

Table 2: Process reactions.[43,44]

	Reaction	
Heterogeneous	$C + 0.5 \cdot O_2 \rightarrow CO$	R1
	$C + CO_2 \leftrightharpoons 2{\cdot}CO$	R2
	$C + H_2O \leftrightharpoons CO + H_2$	R3
	$C + H_2 \leftrightharpoons CH_4$	R4
Homogeneous	$CO + 0.5 \cdot O_2 \leftrightharpoons CO_2$	R5
	$H_2 + 0.5 \cdot O_2 \leftrightharpoons H_2O$	R6
	$CH_4 + 0.5{\cdot}O_2 \leftrightharpoons CO + 2{\cdot}H_2$	R7
	$CO + H_2O \leftrightharpoons CO_2 + H_2$	R8
	$CO_2 + 4{\cdot}H_2 \rightarrow CH_4 + H_2O$	R9
	$CH_4 + H_2O \leftrightharpoons CO + 3{\cdot}H_2$	R10
	$2{\cdot}CO + 2{\cdot}H_2 \rightarrow CH_4 + CO_2$	R11
Tar Cracking	Tars $\rightarrow$ C + C_nH_m + gases	R12
Tar Reforming	$C_nH_m + n{\cdot}H_2O \rightarrow n{\cdot}CO + (n + 0.5{\cdot}m){\cdot}H_2$	R13
	$C_nH_m + n{\cdot}CO_2 \rightarrow 2{\cdot}n{\cdot}CO + (0.5{\cdot}m){\cdot}H_2$	R14
	$C_nH_m + 2{\cdot}n{\cdot}H_2O \rightarrow n{\cdot}CO_2 + (0.5{\cdot}m + 2{\cdot}n){\cdot}H_2$	R15

with higher temperatures in the range of 1150–1250 K, an increase in reaction rates of CH_4 producing reactions is compensated by increasing consuming reactions. Importantly, in all the 4D cases the CH_4 flow increases as a function of time, suggesting that a greater char layer thickness affects the CH_4 production, via methanation or tar cracking reactions (R9–R12).

For the H_2 concentration, it takes between 1000 and 2000 seconds to reach a near steady-state concentration. Increasing the air mass flux and thus the process temperature does not reduce the time, but does increase the value of the near steady-state concentration substantially, mainly influenced by reactions R7 and R8 as well as R12–R15. This initial time suggests that a certain char layer thickness is necessary to promote the release of H_2. Increasing H_2 values at higher flow rates and fuel bed depth suggest that increasing amounts of char downstream of the reaction front as well as higher temperatures increase the release of this product.

The volumetric time-weighted average producer gas constituent concentrations and the calculated HHV of the producer gas at the four different air mass flux configurations for 1D and 4D depth are shown in Figure 6. Very low oxygen concentrations were mea-

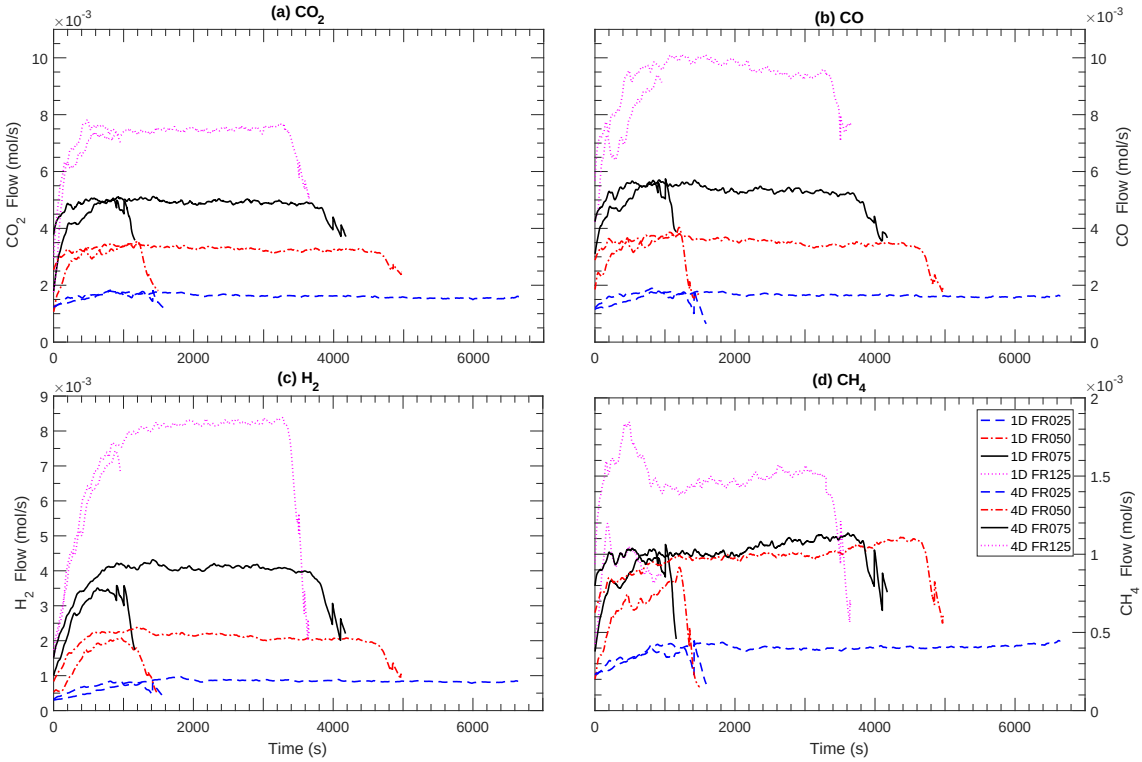

Figure 5: Flow of gaseous devolatilisation products over the period under consideration.

sured in all cases, confirming that the oxygen supply is a reaction limiting variable. All concentrations are notably influenced by the air supply and the fuel bed depth.

The mean concentrations (Figure 6) reflect and clarify the results presented in Figure 5. Although the produced flow of the gaseous products increases, mean CO_2 and CH_4 concentrations decrease in the producer gas with increasing air mass flux, but increase with the fuel bed depth (with the exception of CH_4 in the FR050). At 1D, the CO concentration is similar for all air mass fluxes, while at 4D it increases with the air supply, suggesting an influence of the greater fuel bed depth. The H_2 concentration increases with the air flow for both depths, and by as much as 8 to 14% (vol/vol) at 4D. The trends of both the CO and H_2 concentrations, the main products of tar cracking and reforming reactions, R12–R15, show the combined influence of increasing process temperatures and a greater char layer.

Similar systems have been studied previously with comparable fuels.[20,21] The pro-

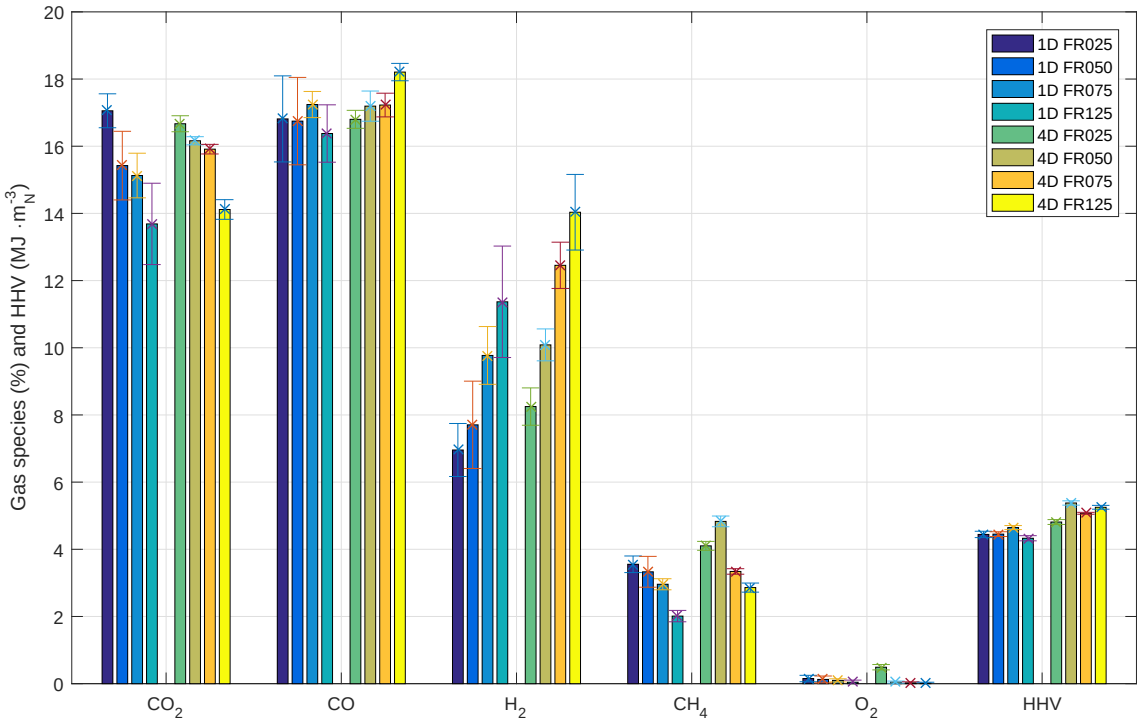

Figure 6: Time-weighted volumetric average concentrations (% vol/vol) of gaseous devolatilisation products at fuel bed depths of 1D and 4D for the different air mass fluxes, as well as the higher heating values of the gas (MJ·m$_N^{-3}$). Error bars indicate the standard error of the mean.

ducer gas composition for similar air mass fluxes has been found to be quite different. Lodgepole pine pellets and Douglas fir chips were tested at 1.6D fuel bed depths. Compared with the results presented here, both fuels produced similar CO and CO_2 concentrations, but lower CH_4 and H_2 concentrations, at an air mass flux of 0.052 kg·m^{-2}·s^{-1}.[21] Wood pellets have also been tested in a 1D depth reactor at air mass fluxes of 0.032 kg·m^{-2}·s^{-1} and 0.051 kg·m^{-2}·s^{-1}. Much lower CO and H_2 concentrations of 8.0% and 1,6% respectively were found at FR032,[20] compared with 16.8% and 7.0% at FR025 1D, as seen in Figure 6. In both cases no thermal insulation of the reactor was used and a resultant 10–20% lower reaction front temperature could be the cause of this discrepancy. Conversely, pine bark chips were tested at higher flow rates and higher reaction temperatures but also exhibited lower concentrations of all gaseous products.[17] A moisture content of >10%, compared with <5% in the used pellets here, will have an influence on this differ-

ence in concentrations, as the moisture evaporation will consume released energy and the greater steam concentration will influence ongoing reactions. Very similar conditions and gaseous concentrations were achieved using Casuarina (*Casuarina equisetifolia*) wood in a thermally insulated reactor.[46] These wide variations in measurements show that small differences in the reactor design or fuel composition can have a significant influence on the producer gas composition and that deeper insights into the batch-fed autothermal conversion process are necessary for efficient reactor design.

3.3.2 Biomass Conversion

Figure 7 presents the molar conversion of biomass carbon (C) into the different products, CO_2, CO, CH_4 and char, with increasing flow rates for both the 1D and 4D cases. "Other" is determined by subtraction and accounts mainly for hydrocarbons (tars) and carbonaceous particles, which were not measured. The amount of carbon converted to "Other" decreases from 34±3% at FR025 to 1.8±1.8% at FR125. This decrease of "Other" products provides an indication of increased tar cracking occurring with a greater air supply and the resulting higher temperatures (§3.2).

At 4D, a greater air supply results in increasing CO_2 and CO yields from 14.2±0.1 to 35.5±4.5%. The increase in CO/CO_2 product ratio at higher air supply rates can be related to carbon oxidation at higher temperatures[45] (see §3.3.1). Furthermore, the char yield decreases by nearly half in the 4D configuration. The increase in the CO and CO_2 yield reflect increasing heterogeneous char gasification (R1–R4) and thus a reduction in char yield. Tar cracking reactions (R12) will also contribute to the increase in gaseous carbonaceous products, mainly of CO.

The conversion to CH_4 shows lower values at FR025 and FR075, and higher at FR050, but the peak value is reached at FR125. A higher air mass flux leads to an increase of the CH_4 and CO gas yields which are the desired species for further gas-phase combustion. This increase in conversion will most likely be the result of increasing tar cracking

reactions due to higher process temperatures with the air supply, as suggested in §3.2.

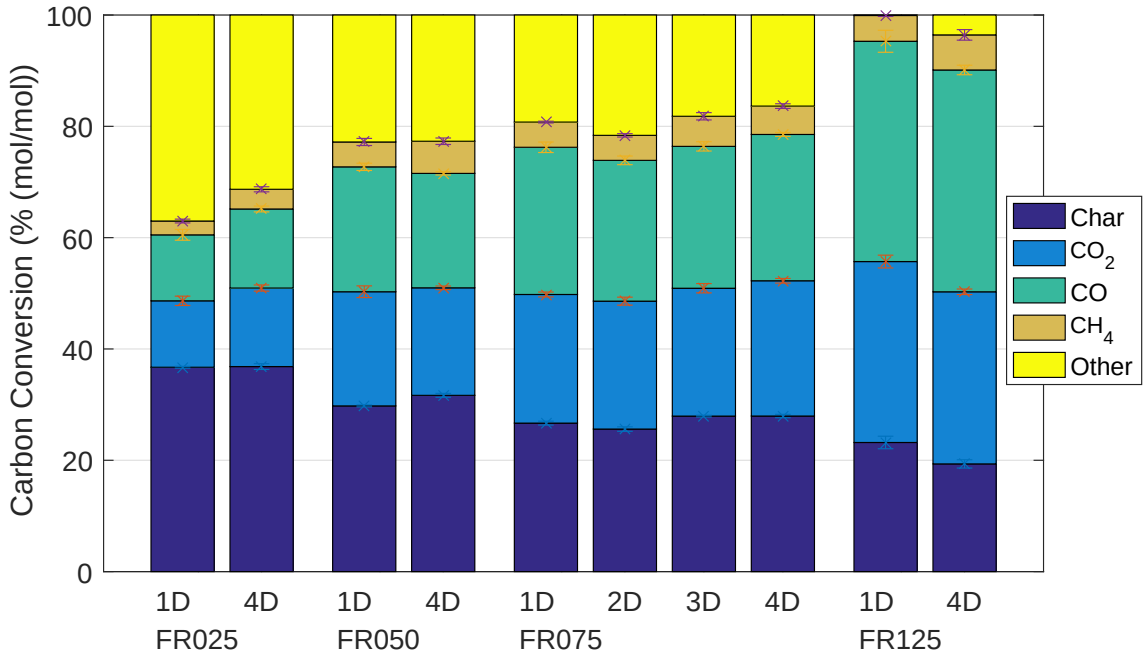

Figure 7: Conversion of initial carbon in the biomass into the different products for increasing flow rates, FR025–FR125, for 1D and 4D fuel bed depths and also at FR075, for 2D and 3D fuel bed depths. Error bars indicate the standard error of the mean.

Figure 8 presents the molar conversion of hydrogen (H) from the biomass into the different hydrogen-containing products. "Other" accounts primarily for water and tars. The H_2 and CH_4 yield increases with the air mass flux. With the air mass flux, the H_2 yield rises from 7.4±1.4 to 35.7±2.7%, from FR025 to FR125. Increasing yields of CH_4 as well as H_2 with rising temperatures are expected (see §3.3.1), due to tar cracking reactions (R12–R15).[28] A trend of increasing hydrogen conversion is visible with the greater fuel bed depth and higher flow rates.

3.3.3 Cold Gas Efficiency

Gasification systems can be evaluated by their cold gas efficiency (CGE), which describes the energy content of the producer gas relative to the energy released from the converted fuel,[47] as per Equation 4. Here, only the measured gases (CO, CO_2, H_2, and CH_4) are considered in the calculation of the CGE: other hydrocarbon species, which have not been

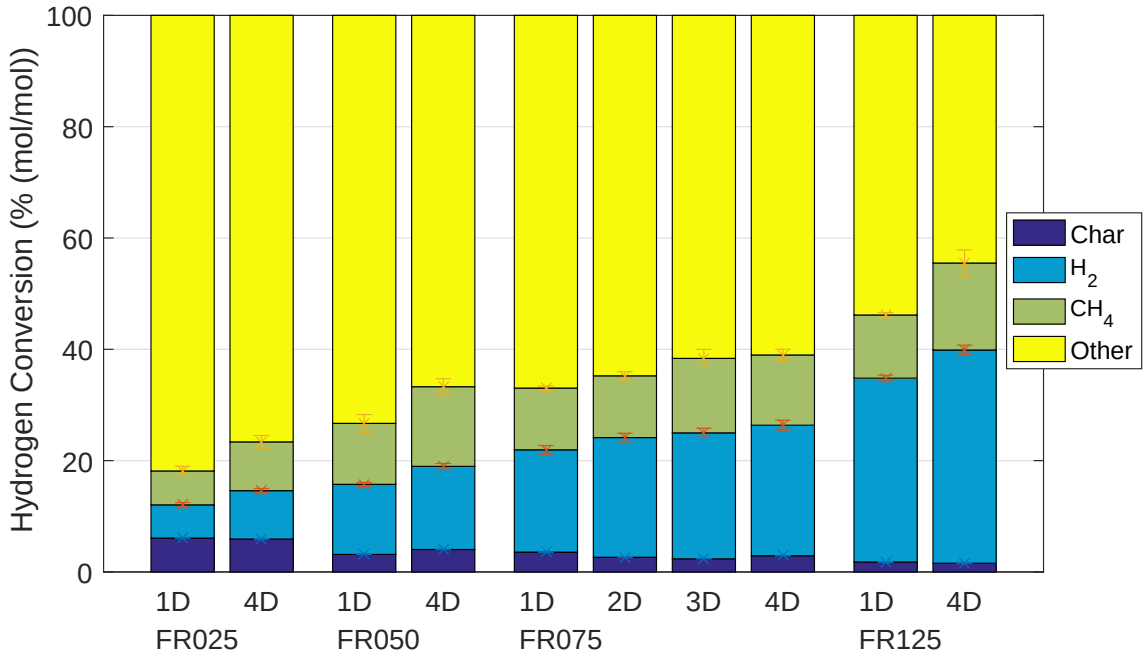

Figure 8: Conversion of the fuel hydrogen into the different products. Error bars indicate the standard error of the mean.

quantified in this study, notably tars, are not included. Statistical analysis suggests significant difference in between FR025-FR050 and FR075-FR125, but in between FR050 and FR075 a lower statistical difference was apparent.

The increased conversion yields of permanent gases, presented in Subsection 3.3.2, are mirrored in the CGE as presented in Figure 9. The CGE increases nearly linearly from 29.3±4.2 to 70.5±2.7% between FR025 and FR125, for 1D and 4D. The low values of the CGE at FR025 can be explained by the high tar content, while at FR125 a large fraction of tars, as well as char, are converted into permanent gases that contribute to the CGE.

Different shapes of *Jacaranda Copaia* wood were used in a similar reactor at air supply rates, approximately 10% lower than FR125, achieving CGE values between 31–38%, which is much lower than the results presented here.[42] In that work it was not stated if char was produced, or also consumed in the process, and how the CGE was calculated, making a direct comparison difficult. In a similar size continuous downdraft gasifier, a CGE over 70% was reported, at an air supply comparable with FR050.[48] Although, the

peak process temperature and the producer gas composition appear similar, the tar yield here seems much higher and the CGE is more than 20% lower.

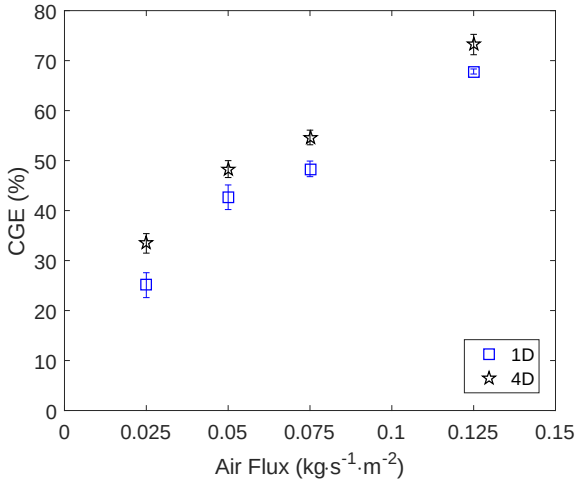

Figure 9: The cold gas efficiency (CGE) as a function the air mass flux for two fuel bed depth. Error bars indicate the standard error of the mean.

3.4 Influence of Fuel Bed Depth

3.4.1 Gaseous Products

Figure 10 presents the temporal evolution of gaseous products for varying fuel bed depths (the average producer gas composition is provided in the Supporting Information). The profiles at 4D and 3D achieve more steady profiles, rather than at 2D and 1D. It is evident that at greater fuel bed depths, the steady propagation of the reaction front occupies a larger part of the process, while at lower fuel bed depths, the effects of transients at start-up and shut-down are more prominent.

In all cases the flow of CH_4 increases as a function of time, suggesting increasing methanation or tar cracking reactions (R9–R12) with a greater char layer thickness (see also §3.3.1). The value of H_2 of the near steady-state flow does not change notably between 2D and 4D. In the 1D configuration the flow remains much lower in the limited time of the process. The time to reach the near steady concentration occupies a larger pro-

portion of the process duration at lower depth. This indicates that a depth greater than 1D is necessary to reach the potential of the H_2 release in this process.

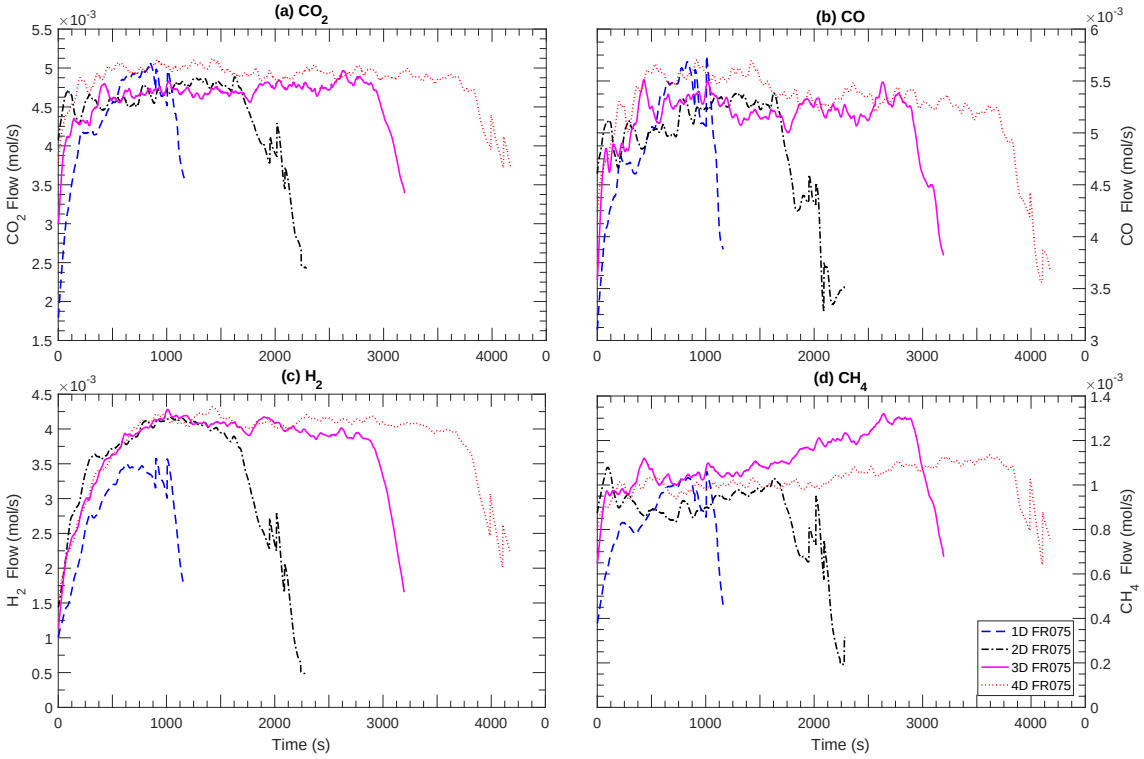

Figure 10: Flow of gaseous devolatilisation products over the period under consideration.

3.4.2 Biomass Conversion

Figure 7 presents the molar conversion of carbon (C) in the biomass into the different products. When comparing the yields with the concentrations, it should be noted that conversion yields consider the species concentration, the process duration and the amount of produced gases, as explained in more detail in Sections 2.5 and 3.3.2. The amount of carbon converted to "Other", mainly tars, decreases from 19.2±1.6 to 16.4±1% between 1D and 4D fuel bed depths, at FR075. This provides an indication of increased tar cracking with greater char layer thickness. A general trend of greater conversion yields of permanent gases and char can be seen at 3D and 4D, when compared with 1D and 2D.

Figure 8 presents the molar conversion of hydrogen (H) in the biomass into the dif-

ferent products. The "Other" species, mainly water and tars, are reduced from 67.0% to 61.0% between 1D and 4D. With depth, there is a change in H_2 yield from 1D to 2D of 18.7 to 21.5%, while it further increases to 23.5% (mol/mol) at 4D. The increase with depth can be related to the temporal profiles, as discussed previously and presented in Figure 5. Cracking of tars, will have an influence on the increase of H_2.

3.4.3 Cold Gas Efficiency

The CGE with increasing fuel bed depth is presented in Figure 11. It can be seen that the CGE increases from 48.4 to 54.6% from 1D to 4D, at FR075. Generally higher efficiencies are achieved at 3D and 4D. These higher efficiencies are the result of greater conversion to combustible permanent gases in the presence of a larger char layer thickness in the system. Statistical analysis confirmed a very low statistic difference between 1D–2D and 3–4D, with much higher difference when comparing 1D and 2D with 3D and 4D.

In the conversion yields in Figure 8 (and in the Supporting Information), where only H_2 shows a substantial increase, the influence of the fuel stack depth seems to have a rather negligible impact on the process. However, the cold gas efficiency in Figure 11 confirms that 1D and 2D are not sufficient and that a quite substantial 10% increase can be achieved when increasing the depth to 3D or 4D.

3.5 Char Layer

Tables 3 and 4 present the mass-based proximate and ultimate analyses, the H:C and O:C ratios, the char product yield and the higher heating value of the produced chars for all configurations. The chars are separated into the top, middle and bottom of the bed for the 4D cases, as explained in Section 2.4. In all cases, the fixed carbon (FC) and the elemental carbon content are very similar, with changing depths and flow rates. All produced chars exhibit a high carbon content, with values greater than 92% for FC and 84% for C.

The volatile matter (VM) as well as the elemental hydrogen content decrease with in-

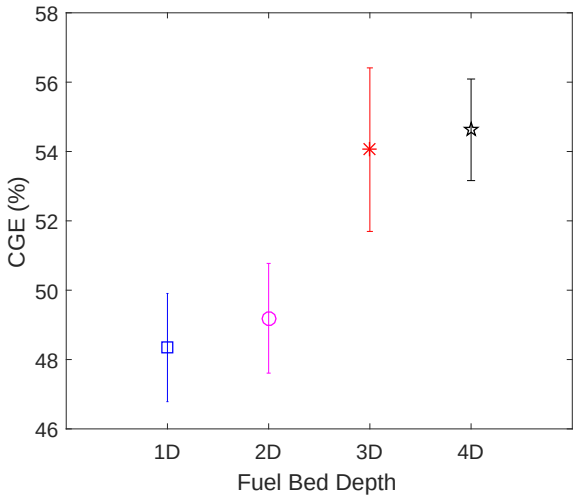

Figure 11: Cold gas efficiency (CGE) over the fuel bed depth at FR075. Error bars indicate the standard error of the mean.

creasing flow rates, as well as fuel bed depths. This trend of reducing elemental hydrogen and hydrogen compounds can be explained by the longer exposure to high temperatures and higher maximum reaction temperatures. A similar behaviour has been established for pyrolysis processes.[49]

In the conversion process the mass-based char yield, as well as the carbon and hydrogen bound in the char, decrease with increasing air mass flux. With increasing fuel bed depth the char yield generally increases which also suggests that char down-stream of the reaction front does not participate in subsequent reactions. At 4DFR025, nearly all FC is retained in the char, while at FR125, only about half is retained.

All produced chars would be regarded as Class 1 biochars based on their CHNO composition, if used as a soil amendment. In all cases the H:C and O:C ratios are much lower than the thresholds proposed by the European Biochar Foundation of 0.7 and 0.4, respectively.[50,51] Generally these ratios are calculated on the basis of the organic carbon (OC) fraction in the char, but because of the high temperatures in this particular conversion process and a carbon fraction of >84% (g/g) for all configurations, all elemental carbon can be assumed to be OC.

Table 3: Proximate and ultimate analyses results for the wood pellet fuel and chars from the different test configurations. Also the H:C, the O:C mass ratios, the char yield with the standard error (SE) and the HHV are shown.

Configuration	FC	VM	Ash	H:C	Yield	HHV
	C	H	N	O:C	SE	MJ/kg
Wood Pellets	17.8	71.5	4.8			17.6
	47.4	6.4	0.1			
1D FR025	93.7	5.4	0.9	0.3	18.6	32.9
	90.3	2.0	0.2	0.06	(0.1)	
1D FR050	94.7	4.5	0.8	0.2	15.0	32.1
	91.2	1.3	0.3	0.06	(0.1)	
1D FR075	93.9	3.4	2.8	0.2	13.8	30.5
	88.4	1.6	0.2	0.08	(0.2)	
1D FR125	95.0	4.2	0.9	0.1	11.9	31.8
	92.0	1.0	0.3	0.05	(0.5)	
2D FR075	95.8	3.6	0.6	0.2	13.9	30.5
	87.7	1.2	0.3	0.09	(0.2)	
3D FR075	85.4	0.7	13.9	0.1	14.3	32.1
	93.3	1.1	0.2	0.04	(0.1)	

Table 4: Proximate and ultimate analyses results for chars from the different test configurations. The H:C and O:C mass ratios, char yield with standard error (SE) and the HHV are also shown.

Configuration	FC	VM	Ash	FC	VM	Ash	FC	VM	Ash	H:C	Yield	HHV
	C	H	N	C	H	N	C	H	N	O:C	SE	MJ/kg
	Bottom			Middle			Top					
4D FR025	94.1	4.6	1.3	94.3	3.7	2.0	94.1	4.1	1.8	0.3	19.9	32.5
	88.7	1.9	0.2	90.2	1.8	0.2	87.5	2.1	0.2	0.08	(0.2)	
4D FR050	95.1	3.5	1.4	94.9	2.9	2.2	96.0	2.5	1.4	0.2	16.6	32.0
	89.4	1.5	0.3	92.3	1.3	0.2	85.2	1.8	0.3	0.08	(0.3)	
4D FR075	93.3	2.7	4.0	92.7	4.2	3.1	93.1	3.7	3.2	0.2	14.4	31.2
	94.3	1.1	0.3	91.6	1.2	0.2	84.7	1.5	0.2	0.07	(0.3)	
4D FR125	94.0	2.4	3.6	85.2	1.9	12.9	88.8	2.8	8.4	0.1	10.1	31.6
	89.7	0.9	0.3	93.3	0.9	0.2	86.0	1.2	0.3	0.07	(0.3)	

3.6 Discussion

The autothermal process in the studied reactor displays an interrelationship of many parameters, such as the air supply, fuel consumption, composition of released products, subsequent exothermic or endothermic reactions of released products and the process temperature. In this process the composition of released products, for a specific fuel, depends mainly on the supply of the oxidiser, but also on internal heat transfer in the fuel as well as external heat loss from the reactor. This complex interrelationship leads to great difficulty in isolating specific influences on the final producer gas composition. Multiple indicators for particular trends in the presented study need further discussion.

When trying to isolate the impact of different influences, it has been observed here that heterogeneous reactions do not seem to occur downstream of the reaction front. The indications for the absence of heterogeneous reactions found in this study are that towards the end of the process, when the char layer thickness is greatest, the flow of carbonaceous products does not increase and a greater fuel bed depths leads to a greater yield of char, except at the highest flow rate. The exception of the highest flow rate supports the argument made in Section 3.1 that this flow rate is a transition between the oxygen- and reaction-limited regimes. Char gasification with CO_2 or H_2O, downstream of the reaction front requires high reactant concentrations as well as high temperatures,[22] which seem only to be present at the highest flow rate. Figure 12 presents the temperature profile in the reactor, from the top (T1) to the bottom (T8) (see Figure 1), for the 4D cases at the time when thermocouple T7 (70 mm above the fuel grate) reaches the maximum temperature. Downstream of the reaction front it can be seen that while for FR125 four thermocouples exceed 800°C, which is considered within the range of gasification processes,[47] this is only the case for one thermocouple for FR075 and none at lower air flow rates. These relatively low temperatures downstream of the reaction front will lead to low reaction rates of char gasification.[45] Furthermore, even at FR125, where the highest temperatures are achieved downstream of the reaction front, it is possible that the increase in hetero-

geneous reactions of the char are due to gasification in the reaction front, with oxygen, rather than downstream with CO_2 or H_2O. Therefore, heterogeneous reactions (R1–R4 in Table 2) downstream of the reaction front can be neglected as possible contributors to increasing conversion yields to permanent gases with depth.

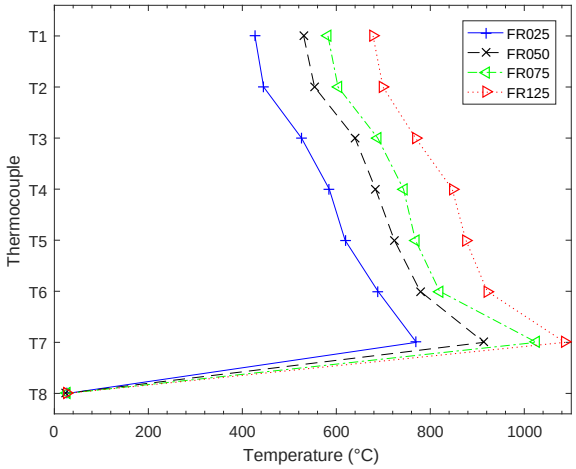

Figure 12: Reactor temperature profile for the 4D cases when thermocouple T7 reaches the maximum temperature.

It can be shown that the conditions in the reaction front do not vary with depth and that heterogeneous reactions do not influence the release of producer gas components downstream. Therefore, the varying producer gas composition and yield with depth could relate to ongoing subsequent processes downstream of the reaction front. Possible downstream reactions, R5–R15, are presented in Table 2. Higher temperatures, as achieved at higher air flow rates, will favour reactants of the exothermic water gas shift and homogeneous methanation reactions, R8–R11, in accordance with *Le Chatelier's* principle, while higher reaction rates for the tar degradation and reforming reactions, R12–R15, are achieved.[52] It can be assumed that the presence of char promotes tar cracking reactions.[44] A greater residence time in the char bed at elevated temperatures (see Figure 12), which results from the propagation of the reaction front down the fuel bed over time, will influence these subsequent reactions. The increase of CH_4 flow, representing all gaseous hydrocarbon species, along the temporal axis as noted in all configurations

(see Figures 5 and 10), supports the assertion of increasing tar cracking reactions in the char layer as it increases in depth. A combination of the reactions, presented in Table 2, will lead to the notable increase in the conversion products H_2, CH_4 and CO, while tar cracking and reforming reactions are most likely to have the greatest influence. Future work on gravimetric determination of the amount of tars and an analysis of the produced species could provide further information.

Experimental investigations on the degradation of tars are generally performed at similar or higher temperatures than the conversion temperature at which the tars are produced. In the present system, thermochemical conversion occurs at the maximum temperature in the reaction front, while degradation is assumed to occur downstream in the char bed at elevated temperatures. The high temperatures in the reaction front will lead to the formation of products that are more thermally stable at these temperatures.[53] Therefore, the limited increase in conversion to permanent gases with increasing fuel bed depths could be partially due to tar cracking, downstream of the reaction front, occurring at lower temperatures than those at which the tars are produced.

One possible application of the new knowledge from this study is in small-scale domestic stoves. In this application, a fuel bed depth of 3D and 4D is expected to lead to a more steady conversion process, with lower tar yields and greater conversion to permanent gases. Tar and permanent gas yields could be influenced by tar cracking reactions in the char bed downstream of the reaction. Furthermore, with a greater fuel bed depth, a longer time is spent in the steady-state propagation of the reaction front, while lower depths are more strongly affected by transients at start-up and shut-down. This could be of particular interest since typically commercial[8] as well as experimental designs of this type of reactor are in the range 1D–2D fuel bed depths, while this research suggests that increasing this parameter has a beneficial effect on the conversion process.

4 Conclusions

The presented study investigates the influence of the air supply and the fuel bed depth on the conversion process in a small-scale batch-fed reverse downdraft reactor. Four flow rates, from 0.025–0.125 $kg \cdot m^{-2} \cdot s^{-1}$, and fuel bed depths, from 100–400 mm (1D–4D), were used in the experiments.

Increasing the air supply also increases the fuel consumption, the temperature and the conversion processes to permanent gases, in the reaction front. Substantially higher combustible gas yields and cold gas efficiencies (CGE) are achieved with higher temperatures at greater air supply levels. With higher temperatures, the increase in combustible gas yields can be explained by greater rates of tar conversion reactions and an increase in the CO/CO_2 product ratio.

When increasing the fuel bed depth, the conditions in the reaction front, such as the fuel consumption and temperatures, are not affected; but it needs to be kept in mind that, as the reaction front moves down the fuel bed, a char layer, of increasing depth, accumulates downstream. It was confirmed that this char layer downstream of the reaction front does not participate in heterogeneous gasification reactions with the gaseous products released from the reaction front. However, conversion of tars appears to be enhanced by a hot char layer leading to increasing concentrations and yields of permanent gases, especially of CO and H_2, with increasing fuel bed depth. For all gaseous products, transients at start-up and shut-down of the process are more dominant at lower fuel bed depths and generally higher conversion to permanent gases can be noted at 3D and 4D, rather than 1D and 2D fuel bed depths. The increase in the permanent gas yield with greater fuel bed depths provides a strong indication that there is a reduction in the release of tars.

The CGE can therefore be improved by increasing the fuel bed depth and even more by providing a greater air supply, or a combination of both. A higher producer gas quality for subsequent combustion applications is achieved with increasing CGE.

For applications in cookstoves, the increase in efficiency with greater fuel depth, larger

than one reactor diameter, could provide a simple tool for optimisation, without compromising on the simplicity of the system. The high efficiency of the investigated process and the potential for further optimisation in combination with the opportunity for the production of high quality biochar make this process especially attractive.

5 Acknowledgements

The authors wish to acknowledge the support of The University of Adelaide and Marc Simpson, the laboratory facilities manager. The contributions to the provision of the experiments by Denver May, Nick Rendoulis, Jack Svetlichny and Matthew Zuill are sincerely appreciated. Thomas Kirch gratefully acknowledges the support provided by the Studienstiftung des Deutschen Volkes.

References

(1) WEC, World Energy Resources: 2013 survey. *World Energy Council* **2013**, 11.

(2) Arora, P.; Jain, S. A review of chronological development in cookstove assessment methods: Challenges and way forward. *Renewable and Sustainable Energy Reviews* **2016**, *55*, 203–220.

(3) Sutar, K. B.; Kohli, S.; Ravi, M. R.; Ray, A. Biomass cookstoves : A review of technical aspects. *Renewable and Sustainable Energy Reviews* **2015**, *41*, 1128–1166.

(4) Reed, T.; Das, A. Handbook of Biomass Downdraft Gasifier Engine Systems. *Solar Energy Research Institute* **1988**, 140.

(5) Martinez, J. D.; Mahkamov, K.; Andrade, R. V.; Silva Lora, E. E. Syngas production in downdraft biomass gasifiers and its application using internal combustion engines. *Renewable Energy* **2012**, *38*, 1–9.

(6) Molino, A.; Chianese, S.; Musmarra, D. Biomass gasification technology: The state of the art overview. *Journal of Energy Chemistry* **2016**, *25*, 10–25.

(7) Reed, T. B.; Larson, R. A wood-gas stove for developing countries. *Energy for Sustainable Development* **1996**, *3*, 34–37.

(8) Roth, C. Micro-gasification : cooking with gas from dry biomass. 2014; `http://www.giz.de/fachexpertise/downloads/giz2014-en-micro-gasification-manual-hera.pdf`.

(9) Karellas, S. In *Biofuels and Biorefineries*; Fang, Z., Ed.; Springer US: Dordrecht, 2015; Vol. 5; Chapter 4, pp 97–117.

(10) Kirch, T.; Medwell, P. R.; Birzer, C. H. Natural draft and forced primary air combustion properties of a top-lit up-draft research furnace. *Biomass and Bioenergy* **2016**, *91*, 108–115.

(11) Kirch, T.; Birzer, C. H.; van Eyk, P. J.; Medwell, P. R. Influence of Primary and Secondary Air Supply on Gaseous Emissions from a Small-Scale Staged Solid Biomass Fuel Combustor. *Energy & Fuels* **2018**, *32*, 4212–4220.

(12) Birzer, C.; Medwell, P.; MacFarlane, G.; Read, M.; Wilkey, J.; Higgins, M.; West, T. A Biochar-producing, Dung-burning Cookstove for Humanitarian Purposes. *Procedia Engineering* **2014**, *78*, 243–249.

(13) Brewer, C.; Brown, R. In *Comprehensive Renewable Energy*; Sayigh, A., Ed.; Elsevier Ltd., 2012; Chapter 5, pp 357–384.

(14) Porteiro, J.; Patiño, D.; Moran, J.; Granada, E. Study of a fixed-bed biomass combustor: Influential parameters on ignition front propagation using parametric analysis. *Energy & Fuels* **2010**, *24*, 3890–3897.

(15) Horttanainen, M.; Saastamoinen, J.; Sarkomaa, P. Operational limits of ignition front propagation against airflow in packed beds of different wood fuels. *Energy & Fuels* **2002**, *16*, 676–686.

(16) Porteiro, J.; Patiño, D.; Collazo, J.; Granada, E.; Moran, J.; Miguez, J. L. Experimental analysis of the ignition front propagation of several biomass fuels in a fixed-bed combustor. *Fuel* **2010**, *89*, 26–35.

(17) Pérez, J. F.; Melgar, A.; Benjumea, P. N. Effect of operating and design parameters on the gasification/combustion process of waste biomass in fixed bed downdraft reactors: An experimental study. *Fuel* **2012**, *96*, 487–496.

(18) Lu, H.; Ip, E.; Scott, J.; Foster, P.; Vickers, M.; Baxter, L. L. Effects of particle shape and size on devolatilization of biomass particle. *Fuel* **2010**, *89*, 1156–1168.

(19) Basu, P. *Biomass Gasification, Pyrolysis, and Torrefaction*, 2nd ed.; Elsevier Inc., 2013.

(20) Varunkumar, S. Packed bed gasification-combustion in biomass based domestic stoves and combustion systems. Ph.D. thesis, Indian Institute of Science, 2012.

(21) Tryner, J.; Tillotson, J. W.; Baumgardner, M. E.; Mohr, J. T.; Defoort, M. W.; Marchese, A. J. The effects of fuel properties , air flow rates , secondary air inlet geometry , and operating mode on the performance of TLUD semi-gasifier cookstoves. *Environmental Science and Technology* **2016**, *50*, 9754 – 9763.

(22) Speight, J. G. *Gasification of Unconventional Feedstock*; Elsevier Inc.: Laramie, 2014; Chapter 2, pp 135–152.

(23) Fitzpatrick, E. M.; Bartle, K. D.; Kubacki, M. L.; Jones, J. M.; Pourkashanian, M.; Ross, A. B.; Williams, A.; Kubica, K. The mechanism of the formation of soot and other pollutants during the co-firing of coal and pine wood in a fixed bed combustor. *Fuel* **2009**, *88*, 2409–2417.

(24) Zhang, Y.; Kajitani, S.; Ashizawa, M.; Miura, K. Peculiarities of rapid pyrolysis of biomass covering medium- and high-temperature ranges. *Energy & Fuels* **2006**, *20*, 2705–2712.

(25) Yu, Q.; Brage, C.; Chen, G.; Sjöström, K. Temperature impact on the formation of tar from biomass pyrolysis in a free-fall reactor. *Journal of Analytical and Applied Pyrolysis* **1997**, *40-41*, 481–489.

(26) Kaltschmitt, M.; Hartmann, H. In *Energie aus Biomasse*, 2nd ed.; Hofbauer, H., Ed.; Springer.

(27) Basu, P. *Biomass Gasification and Pyrolysis*, 2nd ed.; Elsevier Inc., 2013; Chapter 6, pp 177–198.

(28) Milne, T. A.; Evans, R. J.; Abatzoglou, N. Biomass Gasifier "Tars": Their Nature , Formation , and Conversion. *National Technical Information Service (NTIS)* **1998**, 1–68.

(29) Regtop, R. A.; Ellis, J.; Crisp, P. T.; Ekstrom, A.; Fookes, C. J. R. Pyrolysis of model compounds on spent oil shales, minerals and charcoal. Implications for shale oil composition. *Fuel* **1985**, *64*, 1640–1646.

(30) Park, J.; Lee, Y.; Ryu, C. Reduction of primary tar vapor from biomass by hot char particles in fixed bed gasification. *Biomass and Bioenergy* **2016**, *90*, 114–121.

(31) Wu, W. G.; Luo, Y. H.; Su, Y.; Zhang, Y. L.; Zhao, S. H.; Wang, Y. Nascent biomass tar evolution properties under homogeneous/heterogeneous decomposition conditions in a two-stage reactor. *Energy & Fuels* **2011**, *25*, 5394–5406.

(32) Brandt, P.; Larsen, E.; Henriksen, U. High tar reduction in a two-stage gasifier. *Energy & Fuels* **2000**, *14*, 816–819.

(33) Varunkumar, S.; Rajan, N. K. S.; Mukunda, H. S. Experimental and computational studies on a gasifier based stove. *Energy Conversion and Management* **2012**, *53*, 135–141.

(34) Saldarriaga, J. F.; Aguado, R.; Pablos, A.; Amutio, M.; Olazar, M.; Bilbao, J. Fast characterization of biomass fuels by thermogravimetric analysis (TGA). *Fuel* **2015**, *140*, 744–751.

(35) Lenis, Y. A.; Pérez, J. F.; Melgar, A. Fixed bed gasification of Jacaranda Copaia wood: Effect of packing factor and oxygen enriched air. *Industrial Crops and Products* **2016**, *84*, 166–175.

(36) Waldheim, L.; Nilsson, T. Heating value of gases from biomass gasification. *IEA Bioenergy Agreement, Task 20 - Thermal Gasification of Biomass* **2001**, 61.

(37) Bondy, W. H.; Zlot, W. The Standard Error of the Mean and the Difference between Means for Finite Populations. *The American Statistician* **1976**, *30*, 96–97.

(38) Mehta, Y.; Richards, C. Gasification Performance of a Top-Lit Updraft Cook Stove. *Energies* **2017**, *10*, 1529.

(39) Rönnbäck, M.; Axell, M.; Gustavsson, L.; Thunman, H.; Lecher, B. In *Progress in Thermochemical Biomass Conversion*; Bridgwater, A., Ed.; Blackwell Science Ltd: Bodmin, 2001; Chapter 59, pp 743–757.

(40) Baker, E.; Brown, M.; Elliott, D. C.; Mudge, L. Characterization and treatment of tars from biomass gasifiers. *AIChE 1988 Summer National Meeting* **1988**, 11.

(41) Varunkumar, S.; Rajan, N. K. S.; Mukunda, H. S. Universal Flame Propagation Behavior in Packed Bed of Biomass. *Combustion Science and Technology* **2013**, *185*, 1241–1260.

(42) González, W. A.; Pérez, J. F.; Chapela, S.; Porteiro, J. Numerical analysis of wood biomass packing factor in a fixed-bed gasification process. *Renewable Energy* **2018**, *121*, 579–589.

(43) Basu, P. *Biomass Gasification, Pyrolysis and Torrefaction*; Elsevier Inc., 2013; Chapter 7, pp 199–248.

(44) Shen, Y. Chars as carbonaceous adsorbents/catalysts for tar elimination during biomass pyrolysis or gasification. *Renewable and Sustainable Energy Reviews* **2015**, *43*, 281–295.

(45) Laurendeau, N. M. Heterogeneous kinetics of coal char gasification and combustion. *Progress in Energy and Combustion Science* **1978**, *4*, 221–270.

(46) Mahapatra, S.; Kumar, S.; Dasappa, S. Gasification of wood particles in a co-current packed bed: Experiments and model analysis. *Fuel Processing Technology* **2016**, *145*, 76–89.

(47) Higman, C.; Van der Burgt, M. *Gasification*; Elsevier Inc., 2008; Chapter 2, pp 11–31.

(48) Kihedu, J. H.; Yoshiie, R.; Nunome, Y.; Ueki, Y.; Naruse, I. Counter-flow air gasification of woody biomass pellets in the auto-thermal packed bed reactor. *Fuel* **2014**, *117*, 1242–1247.

(49) Williams, P. T.; Besler, S. The Influence of Temperature and Heating Rate on the Slow Pyrolysis of Biomass. *Renewable Energy* **1996**, *7*, 233–250.

(50) Standardized Product Definition and Product Testing Guidelines for Biochar That Is Used in Soil. *International Biochar Initiative* **2015**, 61.

(51) European Biochar Foundation (EBC), Guidelines for a Sustainable Production of Biochar. *European Biochar Foundation (EBC)* **2016**, 1–22.

(52) Morf, P.; Hasler, P.; Nussbaumer, T. Mechanisms and kinetics of homogeneous secondary reactions of tar from continuous pyrolysis of wood chips. *Fuel* **2002**, *81*, 843–853.

(53) Evans, R. J.; Milne, T. A. Molecular characterization of pyrolysis of biomass. 1. Fundamentals. *Energy & Fuels* **1987**, *1*, 123–138.